TCAD Model for Ag-$GeSe_3$-Ni CBRAM Devices

Kiraneswar Muthuseenu
School of Electrical, Computer and Energy Engineering
Arizona State University
Tempe, AZ, USA
kmuthuse@asu.edu

E. Carl Hylin
Silvaco Inc.,
North Chelmsford, MA, USA
carl@hylin.net

Hugh J. Barnaby
School of Electrical, Computer and Energy Engineering
Arizona State University
Tempe, AZ, USA
hbarnaby@asu.edu

Priyanka Apsangi
School of Electrical, Computer and Energy Engineering
Arizona State University
Tempe, AZ, USA
papsangi@asu.edu

Michael N. Kozicki
School of Electrical, Computer and Energy Engineering
Arizona State University
Tempe, AZ, USA
michael.kozicki@asu.edu

Garrett Schlenvogt
Silvaco Inc.,
North Chelmsford, MA, USA
garrett.schlenvogt@silvaco.com

Mark Townsend
Silvaco Inc.,
North Chelmsford, MA, USA
mark.townsend@silvaco.com

***Abstract*— A model for Ag-$GeSe_3$-Ni Conductive Bridge Random Access Memory (CBRAM) device is developed using Technology Computer-Aided Design (TCAD) simulations. A new field-dependent ion mobility saturation model that combines Mott-Gurney ionic transport and a high-field saturation ionic drift velocity model is implemented. Also, an electron mobility model for charge transport through the conductive filament is presented. The model simulates forming and dissolving of the filament at different bias conditions. The simulation results of CBRAM I-V hysteresis curves match well to the experimental data.**

Keywords*— *CBRAM, TCAD, Mott-Gurney model

I. Introduction

CBRAM is an ultra-low power non-volatile memory technology that can be integrated into conventional back-end-of-line (BEOL) CMOS processes [1], [2]. CBRAM have been the subject of extensive research since they provide an ultra-low power alternative to conventional non-volatile memory technologies. When functioning as digital memory, they represent stored data as either a high or low resistance across anode and cathode terminals. CBRAM can also be programed in multi-level or even analog states which makes it a potential technology for artificial synapses in neuromorphic applications [3]. The CBRAM device is a two-terminal metal-electrolyte-metal stack. For the material system considered in this work, the active metal (top) anode is silver (Ag) and the inert metal (bottom) cathode is nickel (Ni). The electrolyte layer is a silver doped chalcogenide glass (Ag-$Ge_{30}Se_{70}$), with a thickness of 70 nm, length of 1µm and width of 10 µm. A thin layer of Ag is dissolved into chalcogenide glass (ChG) using a photo-diffusion process to facilitate ion migration through the glass [4]. The doping profile of Ag in the ChG follows a Gaussian distribution with maximum concentration at the anode/ChG interface. An experimental device with the features above was fabricated at the Arizona State University.

The TCAD device simulator that implements our new CBRAM model is Silvaco's Victory Device Simulator with the Electrochemistry Module. A two-dimensional TCAD structure representative of the fabricated device is shown in Fig. 1. A 2 nm width seed element is added to the top of the Ni cathode in TCAD simulation structure. This enables the formation of the filament from the seed. Without the addition of this seed, a conductive metal sheet will be formed instead of the filament during transient simulation.

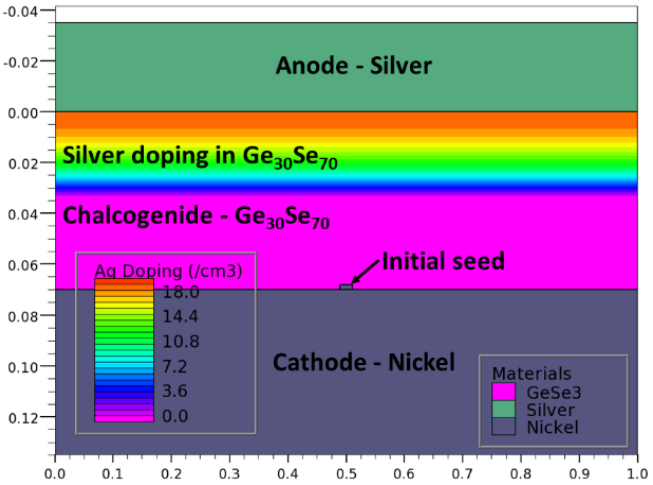

Fig. 1. CBRAM device structure used in this work.

Fig. 2. shows the current-voltage (I-V) hysteresis characteristics of the Ag-$GeSe_3$-Ni CBRAM device fabricated at Arizona State University. The black square curve shows the response of the device for positive anode bias (relative to the cathode potential) and the blue circle curve is the response for negative anode bias.

CBRAM is a type of electrochemical memory that operates via oxidation-reduction reactions. The data stored in the device is set by the resistance between the anode and cathode contacts. In binary operation, the resistance can be switched between a High Resistance State (HRS) and a Low Resistance State (LRS) [1], [2]. Assuming an initial HRS condition, there exists no filament or low resistance pathway between the terminal. When a positive bias is applied to the anode relative to the cathode, the following sequential processes occur: 1) Ag cations (Ag^+) are created through oxidation at the anode/ChG interface (Eq. 1), 2) the cations drift through the electrolyte in the direction of the applied electric field, 3) Ag cations are reduced by gaining an electron at the cathode (Eq. 2). This corresponds to SET process shown in Fig. 2 (inset A).

$$Ag \rightarrow Ag^+ + e^- \quad (1)$$

$$Ag^+ + e^- \rightarrow Ag \quad (2)$$

On continued application of positive bias, a conductive Ag filament grows from the cathode back to the anode. After the application of positive voltage over an appropriate time, the Ag filament will create a conducting bridge between the

978-1-7281-0940-4/19/$31.00 ©2019 IEEE

opposite electrodes through the electrolyte layer. The voltage at which this occurs is called the SET voltage. At this stage, the device switches into LRS (ON state) as shown in Fig. 2 (inset B). The maximum current reached in LRS is set by an externally programmed compliance current that prevents damage to the cell. The device retains the ON state until a sufficient negative bias is applied to the anode. When the polarity of the bias is reversed, Ag ions will drift back to the anode and dissolve the filament. This is called the RESET process (Fig. 2 inset C). Finally, when the filament is fully dissolved the device switches back to HRS (OFF state) as shown in Fig. 2 inset D.

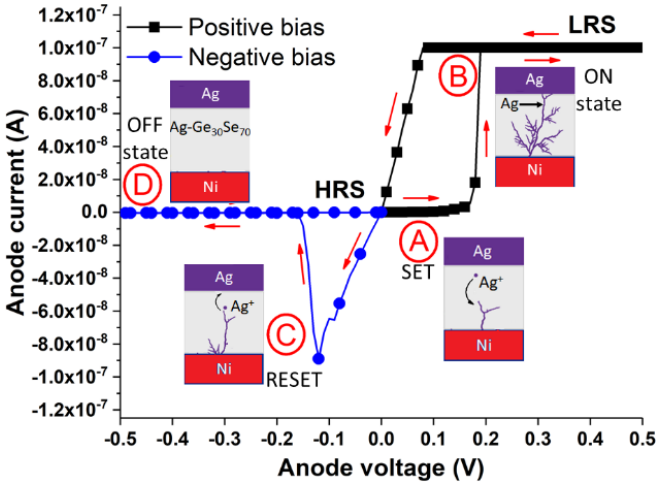

Fig. 2. I-V characteristics of the CBRAM device fabricated at Arizona State University. The insets show different stages of the switching process during the I-V sweep. The compliance current is set at 100 nA.

II. Physical Model

A. Field Dependent Ion Mobility Saturation Model

The field dependent ion mobility of a chemical species is given by the Mott-Gurney model [5]. According to Mott-Gurney, the transport of chemical species in the solid electrolyte (ChG) occurs through ion hopping. The diffusivity, D_S of the chemical species can be expressed as

$$D_S = d_{hop}^2 * v_a * exp\left(\frac{-E_A}{kT_L}\right) * \left(\frac{sinh(\eta_S)}{\eta_S}\right), \quad (3)$$

where d_{hop} and v_a is the hopping distance and the hopping frequency of the species in the ChG layer, respectively [1], [6]. The exponential term corresponds to the probability that the attempted hopping of the species succeeds in overcoming the energy barrier represented by the activation energy E_A. In Eq. 3, k is the Boltzmann constant and T_L is the lattice temperature of the ChG layer. The term η_s can be expressed as [1], [6]

$$\eta_S = \left(\frac{d_{hop}}{2}\right) * z_S * \frac{q}{kT_L} * |E|, \quad (4)$$

where, |E| is the magnitude of the electric field and z_S corresponds to the magnitude and sign of the electric charge on the chemical species S. At large values of η_s, the probability of ion hopping, P_{hop}, in the Mott-Gurney model can be expressed as [6],

$$P_{hop} = exp\left(\eta_S - \frac{E_A}{kT_L}\right). \quad (5)$$

For the CBRAM device discussed here, two chemical species are present: Ag with neutral charge and Ag^+ with a single positive charge. The diffusivity of Ag in ChG layer is negligible compared to Ag^+. The diffusivity parameters of Ag^+ in ChG layer are obtained from [1].

It should be noted that at very high fields, the Mott-Gurney model becomes invalid because the P_{hop} cannot exceed unity. Therefore, at high electric fields the ionic drift velocity saturates at a fraction f_{vsat}, of the thermal velocity. The field dependent ion mobility saturation model implemented in this paper combines the Mott-Gurney model with the high field saturation of the ionic drift velocity. Thus, the diffusivity of the chemical species is revised as [7]

$$D_S = d_{hop}^2 * v_a * exp\left(\frac{-E_A}{kT_L}\right) * \{[\frac{Sinh(\eta_S)}{\eta_S}]^{-2} + [f_{vsat} * \frac{Sinh\left(\frac{E_A}{kT_L}\right)}{|\eta_S|}]^{-2}\}^{-1/2}. \quad (6)$$

The mobility of an ionic species, μ_S, can be related to diffusivity of the species using Einstein relation [6], and is given as

$$\mu_S = z_S * \frac{q}{kT_L} * D_S. \quad (7)$$

Fig. 3. shows the mobility of Ag^+ ions in the ChG layer as a function of electric field. It compares the Ag^+ ion mobility calculated using the Mott-Gurney model and the field dependent ion mobility saturation model. The black square and blue circle symbols correspond to Mott-Gurney model and field dependent ion mobility saturation model, respectively. From the figure it can be observed that the mobility of Ag^+ ions in the ChG layer calculated using Mott-Gurney model will increase rapidly when the magnitude of electric field is approximately $1.1x10^6$ V/cm. The hopping probability exceeds unity at this electric field and therefore Mott-Gurney model is no longer valid above this field. Thus, for high fields the mobility of Ag^+ ion is calculated based on the new field dependent ion mobility saturation model. Using this new model, the mobility of Ag^+ ions peaks at $3x10^{-4}$ $cm^2/V.s$.

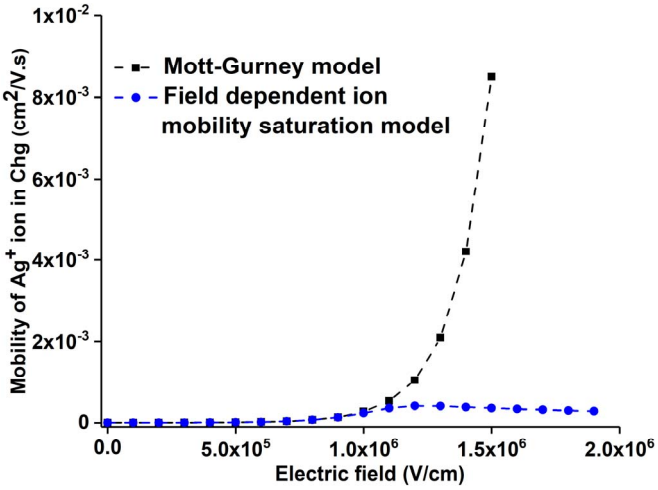

Fig. 3. Plot of mobility Vs electric field for Ag^+ ion in ChG, calculated using Mott-Gurney model and field dependent ion mobility saturation model.

B. *Electron Mobility Model for Filament*

The primary electrochemical reactions occurring in the CBRAM device are given by Eqs. 1 and 2. When the filament starts to form between the cathode and anode, the conductivity of the device increases. As the concentration of the Ag in the filament increases, the electron mobility in the filament increases. Therefore, the total effective electron mobility (μ_{eff}) depends on the electron mobility in ChG layer, electron mobility in the filament and the concentration of the silver in the filament. This electron mobility model is given as [6]

$$\mu_{eff} = \mu_s + w * (\mu_c - \mu_s), \quad (8)$$

where μ_s is the electron mobility in the host layer (ChG), μ_c is the electron mobility in the conductive material (Ag filament) and w is a weight factor that depends on the concentration of the Ag in the conductive filament that can vary between 0 to 1. The weight factor formula is

$$w = \varepsilon + \frac{\left\{(f - f_0) + \delta * ln\left\{cosh\left[\frac{(f - f_0)}{\delta}\right]\right\}\right\}}{2 * (1 - f_0)}, \quad (9)$$

where f is the ratio of local concentration of the conductive bridging species relative to its maximum concentration in the ChG, f_0 is the threshold of bridging species fraction at which the electron mobility starts to increase, δ is the half width of the transition region around f_0, ε is a constant required to make $w = 0$ when $f = 0$.

Fig. 4 compares the electron mobility in the filament as a function of bridging species concentration for different values of f_0 with all the other parameters kept constant. The filled black square, blue circle and red triangle symbols correspond to f_0=0.1, 0.3 and 0.5 respectively. It can be observed that the value of f_0 directly correlates to the local concentration fraction and the conductivity through the filament increases rapidly after this fraction is exceeded. The theory behind this model is that for a local concentration value less than f_0, silver in ChG layer exists in disconnected islands and there is no long-range conduction path between the anode and cathode.

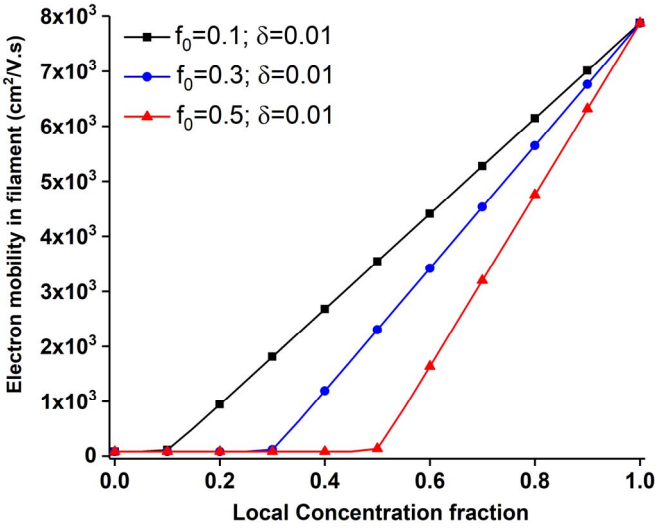

Fig. 4. Mobility of electron in the filament as a function of concentration for different values of f_0 when δ=*0.01*.

Fig. 5 compares the electron mobility in the filament for different values of δ and f_0=0.3.The unfilled black square, blue circle and red triangle symbols correspond to δ=0.01, 0.05 and 0.1, respectively. As can be observed from Fig. 5, the electron mobility in the filament increases more gradually as the δ value is increased.

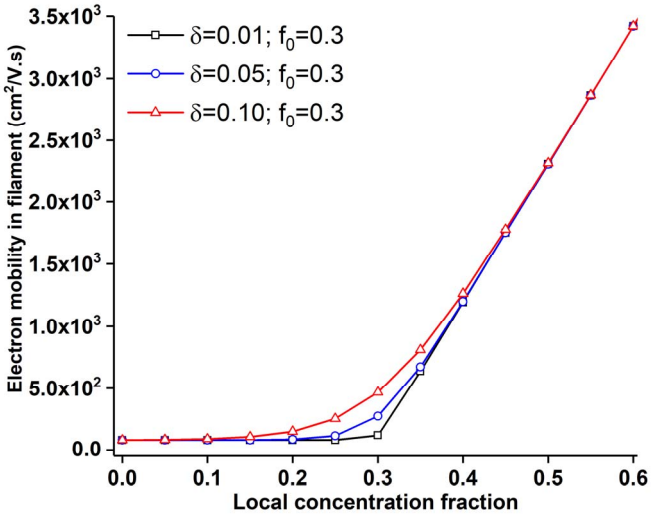

Fig. 5. Mobility of electron in the filament as a function of concentration for different values of δ=*0.01* when f_0=0.3.

III. Simulation Results

Fig. 6 shows TCAD simulations of the forming and dissolving of the Ag filament at different biases during the I-V hysteresis sweep. It can be observed that the concentration of Ag is being modulated in the horizontal center of the device where the seed element was added. In the initial condition with 0V, no filament is present in the device and the device is in HRS as shown in Fig. 6 (inset A). When a 0.5V is applied to the anode, a full Ag filament is formed between the cathode and anode as can be seen in Fig. 6 (inset B). The concentration of Ag throughout the filament is on the order of 10^{20}-10^{21}cm^{-3}. When the voltage applied is ramped down to 0V (inset C), the device retains the filament in the ChG layer, though the concentration of Ag near the anode drops to 10^{19}cm^{-3}. When -0.5V is applied to the anode (inset D), the filament is fully dissolved, and the device goes to HRS.

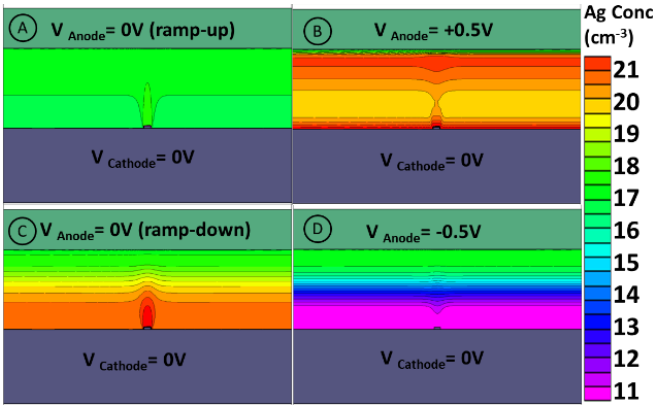

Fig. 6. Concentration of silver at different biases during the I-V hysteresis sweep.

Fig. 7 compares experimental data and simulation results of the I-V hysteresis sweep performed on a Ag-$Ge_{30}Se_{70}$ CBRAM device. Unlike Fig. 2, the curves in Fig. 7 plot log current magnitude vs. linear voltage. The filled black squares and unfilled blue circle symbols correspond to the experimental data and TCAD simulation results, respectively.

In Fig. 7 the region of the sweep labeled (1) corresponds to ramping up of the anode voltage from 0V to 0.5. Sweep region (2) corresponds to ramping down the anode voltage from 0.5V to 0V. Region (3) corresponds to the ramping down of voltage from 0V to -0.5. Region (4) corresponds to ramping up of voltage from -0.5V to 0V. The silver filament is formed in region (1), i.e., the device is switched from HRS to LRS. The filament is dissolved in region (3), i.e., the device is switched from LRS to HRS. A reasonably close fit between the experimental data and TCAD simulation can be observed.

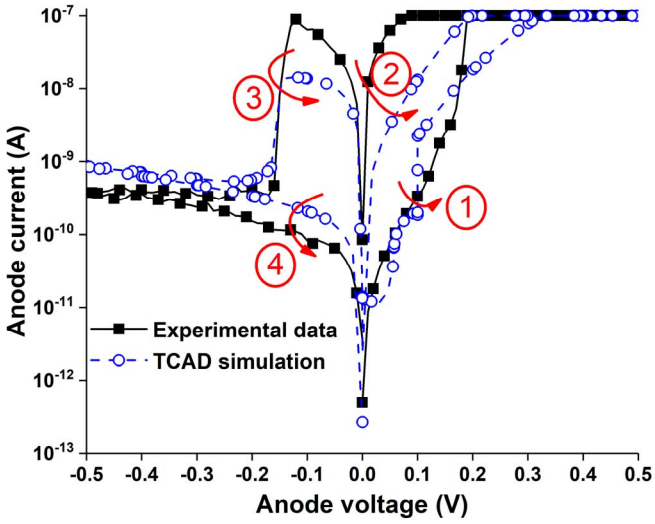

Fig. 7. Comparison of experimental data and simulation results of an I-V hysteresis sweep. The compliance current is set at 100 nA.

Fig. 8. plots the SET voltage for different ramp-rates, simulated using the TCAD model. For our purposes, we define the SET voltage as the voltage at which the current reaches 100 nA during I-V forward sweep. This relationship between ramp-rate and SET voltage was reported experimentally in [8], providing further validation of the model.

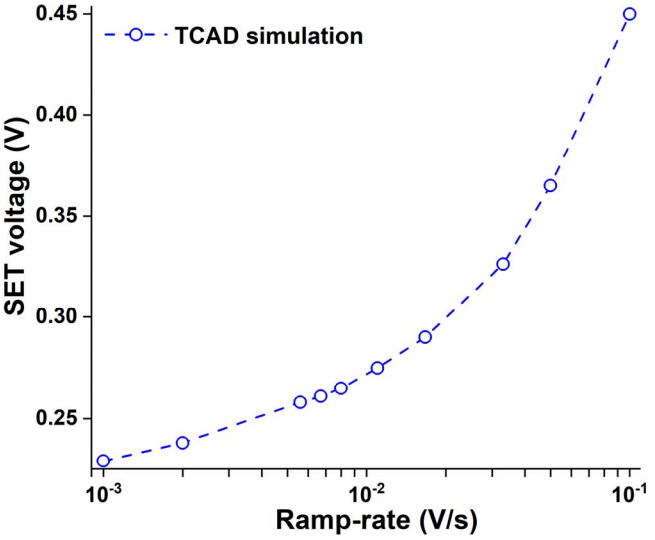

Fig. 8. Simulation results of SET voltage vs. ramp-rate.

IV. Conclusion

This paper presents modeling results which reproduce the formation and dissolution of filaments in CBRAM devices. This is the first time the CBRAM has been modelled in a commercial TCAD device simulator tool. The simulator implements new model for the transport of charged species in the ChG layer. The field dependent ion mobility saturation model presented in this paper combines the Mott-Gurney model and high field saturation of the ionic drift velocity model. At high fields, when the hopping probability in Mott-Gurney model exceeds unity, the diffusivity of the chemical species saturates at a fraction of thermal velocity. The second model described in this paper calculates the mobility of the electrons in the filament as a function of bridging species concentration. This model assumes that below a certain threshold of bridging species concentration, the species are present in the ChG layer as disconnected islands and no long-range conduction path exists between anode and cathode. After the species concentration exceeds the threshold, a linear increase in the conductivity through the filament is implemented by the model. The above two models have been implemented using the electrochemistry module in Silvaco's Victory device simulator. Comparison of I-V hysteresis characteristics between the simulations and the experimental data shows good agreement.

Acknowledgment

This work was funded in part by DTRA under grant no. HDTRA1-17-1-0038 and Arizona State University Nanofab which is supported by NSF award number NNCI – 1542160.

References

[1] M. N. Kozicki and H. J. Barnaby, "Conductive bridging random access memory - Materials, devices and applications," *Semicond. Sci. Technol.*, vol. 31, no. 11, 2016.

[2] M. N. Kozicki, M. Park, and M. Mitkova, "Nanoscale memory elements based on solid-state electrolytes," in *IEEE Transactions on Nanotechnology*, 2005.

[3] G. Indiveri, B. Linares-Barranco, R. Legenstein, G. Deligeorgis, and T. Prodromakis, "Integration of nanoscale memristor synapses in neuromorphic computing architectures," *Nanotechnology*, 2013.

[4] M. N. Kozicki and M. Mitkova, "Mass transport in chalcogenide electrolyte films – materials and applications," *J. Non. Cryst. Solids*, vol. 352, no. 6–7, pp. 567–577, May 2006.

[5] N. F. Mott and R. W. Gurney, *Electronic processes in ionic crystals; 2nd ed.* Oxford University Press, 1948.

[6] *Victory Device User's Manual*. Silvaco Inc. USA.

[7] J. Habasaki, C. Leon, and K. L. Ngai, *Dynamics of Glassy, Crystalline and Liquid Ionic Conductors*. 2017.

[8] C. Schindler, G. Staikov, and R. Waser, "Electrode kinetics of Cu–SiO2-based resistive switching cells: Overcoming the voltage-time dilemma of electrochemical metallization memories," *Appl. Phys. Lett*, vol. 94, p. 72109, 2009.